

Distributed and heterogeneous tensor–vector contraction algorithms for high performance computing^{*,**}

Pedro J. Martinez-Ferrer^{a,b,*}, Albert-Jan Yzelman, Vicenç Beltran^b

^a*Departament d'Arquitectura de Computadors (DAC), Universitat Politècnica de Catalunya - BarcelonaTech (UPC), Campus Nord, Edif. D6, C. Jordi Girona 1-3, Barcelona, 08034, Catalunya, Spain*

^b*Barcelona Supercomputing Center (BSC), Pl. Eusebi Güell 1-3, Barcelona, 08034, Catalunya, Spain*

Abstract

The tensor–vector contraction (TVC) is the most memory-bound operation of its class and a core component of the higher-order power method (HOPM). This paper brings distributed-memory parallelization to a native TVC algorithm for dense tensors that overall remains oblivious to contraction mode, tensor splitting and tensor order. Similarly, we propose a novel distributed HOPM, namely dHOPM₃, that can save up to one order of magnitude of streamed memory and is about twice as costly in terms of data movement as a distributed TVC operation (dTVC) when using task-based parallelization. The numerical experiments carried out in this work on three different architectures featuring multi-core and accelerators confirm that the performances of dTVC and dHOPM₃ remain relatively close to the peak system memory bandwidth (50%–80%, depending on the architecture) and on par with STREAM benchmark figures. On strong scalability scenarios, our native multi-core implementations of these two algorithms can achieve similar and sometimes even greater performance figures than those based upon state-of-the-art CUDA batched kernels. Finally, we demonstrate that both computation and communication can benefit from mixed precision arithmetic also in cases where the hardware does not support low precision data types natively.

Keywords:

tensor contraction, distributed memory, high bandwidth memory, mixed precision, GPU, task-based parallelization

1. Introduction

Tensors can be considered as multidimensional arrays that store data in a certain manner according to multiple (i.e., multilinear) attributes. Exploiting them is of great importance since it allows to extract patterns inherently present in such datasets. It is the field of multilinear algebra that defines tensor operations and algorithms such as products, transformations, and decompositions to name but a few [1]. A major kernel is the tensor contraction, which includes the following operations: (i) tensor–tensor contraction (TTC), (ii) tensor–matrix contraction (TMC), and (iii) tensor–vector contraction (TVC), being all of them core components in widely used tensor algorithms: the Khatri-Rao product [2], the higher-order orthogonal iteration (HOOI) algorithm [3] that computes the truncated Tucker decomposition [4], the alternating least squares

(ALS) algorithm for the canonical polyadic decomposition (CPD) [5], or the higher-order power method (HOPM) [3].

While TMC or TTC imply the contraction over two or more modes of a given input tensor, TVC performs a contraction over one single mode, rendering it a true bandwidth-bounded kernel. In fact, TVC attains a mere arithmetic intensity between 1 and 2 FLOP/byte. Therefore, it comes as no surprise that the TVC performance is often measured in terms of memory bandwidth (GB/s) while, in the case of TMC and TTC operations, the throughput is typically given in GFLOP/s, in analogy to what occurs with the equivalent linear algebraic operations: matrix–vector multiplication (MVM) and matrix–matrix multiplication (MMM), respectively. This contribution focuses exclusively on the performance of the TVC on distributed systems and a more complex tensor algorithm such as the HOPM.

The actual computation inside a TVC kernel can be achieved in different ways, e.g. via the “looped” and “unfolded” algorithms. Both of them appeal to the use of MVM operations, which requires the conversion of the input tensor into its matricized form before the actual contraction takes place. While the looped variant recognizes the input tensor as a series of contiguous matrices and carries out several MVMs, the unfolded counterpart first needs to reorganize the tensor in memory, at the expense of additional data movement, in order to assemble a single

*©2025. This manuscript version is made available under the CC BY-NC-ND 4.0 license <https://creativecommons.org/licenses/by-nc-nd/4.0/>

**Published journal article available at <https://doi.org/10.1016/j.future.2024.107698>

*Corresponding author

Email addresses: pedro.martinez.ferrer@upc.edu (Pedro J. Martinez-Ferrer), albert-jan@yzelman.net (Albert-Jan Yzelman), vbeltan@bsc.es (Vicenç Beltran)

large matrix and conduct one unique MVM. The popularity of these two approaches resides in the fact that they rely upon a broadly available and optimized BLAS level 2 routine: `gemv`. Nevertheless, TVC is far more susceptible to mode-awareness —thus indicating that performance is strongly influenced by the contraction mode k — than a regular second-order contraction: either vector–matrix ($k = 0$) or matrix–vector ($k = 1$) multiplication. Indeed, in a shared-memory parallel context, it may not be possible to evenly distribute MVMs among available threads in the looped TVC algorithm, resulting in suboptimal performance [6]: up to 18% lower performance and up to 71% higher variability across contraction modes. For this reason, authors have recently begun paying attention to mode-oblivious TVC procedures [6, 7, 8].

With the increasing volumes of big data necessary to feed the training models used in the field of artificial intelligence, it becomes necessary to provide fast and, more importantly, scalable implementations of tensor operations [9]. Distributed implementations of TVC and HOPM must execute efficiently on modern and advanced high performance computing (HPC) systems composed of clusters of multicore and manycore central processor units (CPUs), graphics processor units (GPUs), and high bandwidth memory (HBM) such as those currently found on pre-exascale systems and future exascale systems. On this matter, particular attention must be paid to the streamed memory (i.e., the total amount of touched memory) and communication performance of such distributed algorithms, as well as their overall memory utilization and possible synchronization overheads.

This paper constitutes an extension over our previous article on a shared-memory, native TVC algorithm for dense tensors [8]. In this work, we tackle the parallel performance of distributed-memory TVC and HOPM algorithms by:

- Developing distributed-memory, highly optimized TVC and HOPM algorithms and rendering them publicly available in an open-source library [10].
- Providing analytical formulae to assess the effect of one-dimensional MPI splitting on the streamed memory of TVC and HOPM algorithms.
- Carrying out exhaustive numerical experiments of distributed TVC and HOPM over all contraction and splitting modes using different parallel paradigms and three architectures featuring CPUs, GPUs and high bandwidth memory.
- Assessing the performance of distributed TVC and HOPM against state-of-the-art kernels and tensor libraries as well as theoretical bandwidth values for single and ad-hoc, mixed precision kernels.

The remainder of this paper is organized as follows. Sections 2 and 3 are dedicated to giving some related work and describing basic aspects about tensors. In Section 4 we detail our distributed TVC and HOPM algorithms. We

carry out our numerical experiments in Section 5 to assess the performance of the aforementioned algorithms and, finally, Section 6 presents the final conclusions and future work.

2. Related work

There are numerous examples of tensor–vector contraction algorithms, the majority of them being based upon BLAS level 2 and 3 routines [11, 12]. Consequently, it is not rare that such algorithms heavily exploit HPC libraries such as Intel oneMKL, OpenBLAS [13], BLIS [14], as well as LIBXSMM [15] which provides better performance over repetitive small matrix–matrix multiplications. One of the main challenges of TVC, besides of its memory-bound nature, is its performance reliance on the contraction mode. As a result, its global efficiency can be compromised even with highly optimized BLAS routines. Pawłowski et al. introduced a sequential, mode-oblivious TVC algorithm based on the Morton-ordered memory layout [6] and later parallelized it on shared-memory systems [7]. In this respect, we recently proposed a shared-memory, mode-oblivious native TVC algorithm for nonhierarchically stored dense tensors [8] that naturally distributes the column space of the matricized view of a tensor among CPU cores thereby resulting in a specialized, *nonstandard* BLAS level 2 routine.

With the advent of big data analysis, it has become necessary to perform tensor calculations on large scale, distributed systems. Existing tensor libraries typically fall within two main categories. In the first category, the actual distribution takes place at the filesystem level via the “mapReduce” programming paradigm popularized by Hadoop, e.g. GigaTensor [16] and BIGtensor [17], as well as Spark, e.g. CSTF [18]. In general, these distributed implementations do not support higher-order tensors and require additional tensor unfolding operations owing to the explicit parallel distribution which, in the end, result in filesystem overhead. The second category is more interesting from a HPC perspective with applications making extensive use of the MPI library [19]. The Algebraic Programming (ALP) framework¹ leverages explicit algebraic annotations to computations for optimization and auto-parallelization, both shared- and distributed-memory. ALP/GraphBLAS and the wider GraphBLAS efforts promote the paradigm for generalized sparse linear algebra [20, 21], whereas ALP/Dense adds dense linear algebra support [22]. Remarkable examples of tensor frameworks for distributed systems are CTF [23] and tiledArray [24], both achieving similar levels of parallel performance, as well as Deinsum/DaCe [25]. CTF aims at minimizing communication cost, rather than necessarily achieving best performance. Its flexibility for multidimensional tensor splitting implies data redistribution (copying and transposition), hence giving rise to very

¹Visit: <https://algebraic-programming.github.io/>

low flop-to-byte ratio algorithms that may not achieve memory bandwidth peak performance. Both CTF and tiledArray resort to batched BLAS primitives (e.g. from LAPACK [26], ScaLAPACK [27] and others cited above) with the aforementioned implications on looped TVC performance. All things considered, the main advantage offered by these two frameworks resides in the simplicity and generality of expressing tensor operations via a domain-specific language (DSL). On the other hand, Deinsum translates Python code into high performance binaries, derives data movement-optimal tiling, generates corresponding distributed schedules, and can optimize the performance of local computations by increasing their arithmetic intensity, demonstrating significant speedups over CTF.

To the best of our knowledge, there are no previous works focusing on the performance of a mode-oblivious TVC algorithm on distributed systems using higher-order dense tensors and evaluating the effects of tensor splitting on bandwidth from both analytical and numerical perspectives. Moreover, no other BLAS level 2 TVC algorithm with oblivious properties has been proposed for hybrid computing, or compared against state-of-the-art tensor libraries for distributed systems, or tailored GPU kernels for heterogeneous computing. In this regard, the present work showcases the importance of seeking near theoretical bandwidth performance during distributed TVC operations, making special emphasis on a real-world tensor operation: the distributed higher-order power method. We hope that our contribution will be used as an example of future development around HPC libraries oriented towards tensor operations on distributed and heterogeneous systems.

3. Background

We briefly introduce some basic concepts about tensors taken mainly from Kolda & Bader [1] and reuse the notation introduced in our previous work [8]. The font shapes x , \mathbf{x} , \mathbf{X} and \mathcal{X} refer to scalars, vectors, matrices, and tensors, respectively. We interpret dense tensors as multidimensional arrays stored in system memory following a last-order, nonhierarchical storage layout (see Fig. 1) which is indeed equivalent to the multidimensional array ordering used by the C/C++ programming languages. Similarly to these languages, we adopt a zero-based indexing.

By definition, a d -order tensor $\mathcal{A} \in \mathbb{R}^{n_0 \times n_1 \times \dots \times n_{d-1}}$ is composed of d distinct modes of size n_i and accounts for a total of $N = \prod_{i=0}^{d-1} n_i$ elements. The k -mode contraction ($0 \leq k \leq d-1$) of the previous tensor against a given vector $\mathbf{x} \in \mathbb{R}^{n_k}$ can be written as $\mathcal{Y} = \mathcal{A} \times_k \mathbf{x}$. The resulting tensor, $\mathcal{Y} \in \mathbb{R}^{n_0 \times \dots \times n_{k-1} \times n_{k+1} \times \dots \times n_{d-1}}$, is composed of only $d-1$ modes: its supposedly k -th mode remains of size unity as a result of the contraction.

For the actual computation of the previous TVC it is practical to reinterpret the input tensor \mathcal{A} in matrix form. By defining $u = \prod_{i=0}^{k-1} n_i$ and $v = \prod_{i=k+1}^{d-1} n_i$ one can build

the matricized form of such tensor $\mathbf{A}^{u \times v \times n_k}$ and its transpose $\mathbf{A}^{n_k \times uv}$. Now a looped TVC algorithm can be built upon a series of classical matrix–vector multiplications over contiguous subsets of \mathbf{A} . The kind of operation depends on the memory layout and, for the last-order arrangement adopted herein, one single matrix–vector multiplication, $\mathcal{Y} = \mathbf{A}^{u \times n_k} \times_k \mathbf{x}$ is required for the last contraction mode $k = d-1$; otherwise, u independent, equally-sized, left-hand sided vector–matrix multiplications of the form $\mathcal{Y} = \mathbf{x}^\top \times_k \mathbf{A}^{n_k \times v}$ are necessary for the remaining modes $k < d-1$. Note that $u = 1$ for $k = 0$ and $v = 1$ for $k = d-1$.

The sequential looped algorithm described above has been widely adopted by tensor libraries and can be parallelized at two levels: (i) the matrix–vector (or vector–matrix) multiplication itself and/or (ii) the u independent multiplications for $0 < k < d-1$. HPC libraries such as Intel oneMKL and NVIDIA cuBLAS already provide optimized (i.e., batched) functions [28] for subsequent MVMs: `cblas_gemv_batch_strided` for the former and `cublas_gemvStridedBatched` for the later. Nevertheless, all these efforts do not prevent this looped algorithm, either in its sequential or parallel version, from being exposed to mode-aware, suboptimal performance and, therefore, it becomes necessary to find alternative approaches to the looped TVC.

The higher-order power method is a generalization of the well-known power iteration algorithm applied to matrices and is employed to find the best rank-1 approximation of a tensor [3]. Given a d -order input tensor \mathcal{A} and a set of d compatible vectors $\mathbf{x}_0, \mathbf{x}_1, \dots, \mathbf{x}_{d-1}$, the HOPM performs d external iterations within which $d-1$ TVC operations are carried out consecutively omitting, precisely, the contraction along the external mode. This results in a total of $d(d-1)$ tensor contractions, which renders the HOPM algorithm an excellent benchmark for testing the performance of different TVC implementations. We refer the reader to Refs. [3, 6] for a canonical representation of the HOPM algorithm.

It is worth mentioning that the tensor operations described in this section refer basically to sequential algorithms. Shared-memory, parallel implementations of TVC are discussed by Pawłowski et al. [7] and can also be found in our previous work [8]. Distributed-memory implementations are addressed in the next section.

4. Distributed algorithms

This section firstly introduces the dTVC and discusses the particularities of tensor splitting on distributed systems during tensor–vector contractions and, secondly, it proposes an optimized version of the dHOPM. Finally, it comments on the data-flow parallelization strategy adopted for the dHOPM based on task annotations.

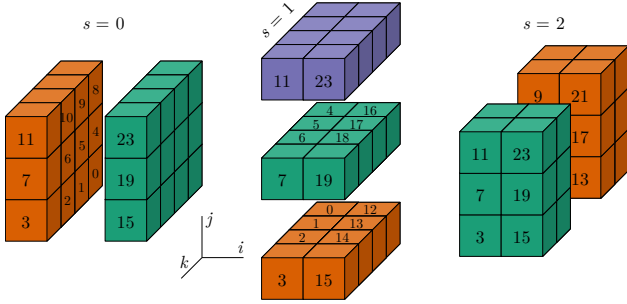


Figure 1: One-dimensional optimal splittings ($s = 0, 1, 2$) using up to three processes ($p = 3$) for a third-order tensor $\mathcal{A}^{2 \times 3 \times 4}$ stored in last-order, nonhierarchical memory layout.

4.1. Distributed-memory tensor–vector contraction

To allow for distributed-memory TVC computations, one can split the given input tensor \mathcal{A} along one or more dimensions. Such splitting also influences the output tensor \mathcal{Y} that is distributed in a similar manner. The input vector \mathbf{x} that participates in the contraction can be harmlessly duplicated among the p distributed processes since, in general, we can assume that $uv \gg n_k$. In this work, we only consider one-dimensional cuts of both the input and output tensors for three main reasons: (i) it yields minimum communication [7], (ii) it gives best computational performance as it does not incur additional tensor unfolding operations, and (iii) it greatly simplifies tensor distribution and reassembly. The major disadvantage of 1D splitting resides in the fact that the maximum number of processes that can be used is determined by $\max(n_i)$. Such processes can be bound to CPU cores, NUMA nodes, GPU devices or even entire compute nodes thereby maximizing the potential for parallelism.

Let us define the contraction mode k and splitting dimension s . Since we store tensors in last-order layout, a splitting along the first dimension of \mathcal{A} guarantees the contiguity between elements of the resulting $\mathcal{A}^{(p)}$ distributed subtensors: $\mathcal{A} = \bigsqcup_p \mathcal{A}^{(p)}$ with $\mathcal{A}^{(p)} \in \mathbb{R}^{[n_0/p] \times n_1 \times \dots \times n_{d-1}}$. In other words, the distributed tensors can be reassembled into a global tensor straightforwardly as shown in Fig. 1 with $s = 0$. The symbol \bigsqcup_p indicates the disjoint union of p tensors and the brackets in $[n_0/p]$ refer to the *optimal* division between n_0 and p . Usually, it corresponds to the ceiling division $\lceil n_0/p \rceil$ although, for *vectorization* purposes, we employ a heuristic technique that seeks to promote quotients that are multiple of the vector length (e.g., 512 bits). This may override (i.e., lower) the value of p for an optimal splitting; for instance, Fig. 1 with $s = 2$ results in $[4/3] \rightarrow 4/2$, that is $p \rightarrow 2$, so that only two of the three requested processes are actually employed. Following the same reasoning, a cut along the last dimension, $[n_{d-1}/p]$, results in the most indirect tensor distribution and later assembly: in the particular case of a second-order tensor, this corresponds to splitting along columns ($s = 1$) a matrix stored in row-major memory layout.

We now proceed with the tensor–vector contraction

algorithm in terms of both intra- and inter-process data movement. A general, BLAS-like expression for the distributed TVC operation with typical scalars α and β can be written for $k \neq s$ as

$$\mathcal{Y} := \alpha \bigsqcup_p \mathcal{A}^{(p)} \times_{k \neq s} \mathbf{x} + \beta \bigsqcup_p \mathcal{Y}^{(p)}, \quad (1)$$

otherwise

$$\mathcal{Y} := \alpha \sum_p \mathcal{A}^{(p)} \times_{k=s} \mathbf{x}^{(p)} + \beta \bigsqcup_p \mathcal{Y}^{(p)}, \quad (2)$$

when the contraction mode and the splitting dimension coincide ($k = s$). This second case remains suboptimal because each distributed TVC operation yields p subtensors with the exact same size N/n_k as the global result, which translates into more local computations and hence streamed memory compared to the first case. Additionally, Eq. (2) demands a collective summation of all these equally-sized subtensors, element by element, to get the global tensor, hence the sum symbol. In contrast, Eq. (1) incurs much less communication because each subtensor only consists of approximately $N[n_s/p]/(n_k n_s) \approx N/(n_k p)$ elements. Since $k = s$ leads to further communication as well as computation, one should avoid contracting tensors along their splitting dimension as much as possible. What is more important, it is strongly encouraged to work with the distributed output tensors and only construct the global tensor when strictly needed because communication is slow and available memory may also be an issue. Finally, $\mathbf{x}^{(p)}$ in Eq. (2) indicates that the contraction operates on a disjoint subset of \mathbf{x} instead of the entire vector. Getting back to the previous matrix analogy, Eq. (2) is identical to a series of matrix–vector multiplications applied to subsets of both \mathbf{x} and \mathbf{A} , where the matrix is distributed along columns ($k = s = 1$) or a series of vector–matrix multiplications when the matrix is distributed along rows ($k = s = 0$).

An important aspect related to the global construction of the output tensor is the contiguity of the elements being assembled. As previously shown in Fig. 1, using the last-order layout with $s = 0$ simply requires to contiguously gather all rows from each process in order to build the global tensor. On the other hand, for $s > 0$ it becomes necessary to communicate fragments of data from each distributed tensor and interleave them inside the global tensor. To this end, one can resort to the matricized views of $\mathcal{Y}^{(p)}$ and \mathcal{Y} , both split along the $s - 1$ dimension, to determine the groups of columns to be collected from each process. This results in $w = \prod_{i=0}^{s-2} n_i$ communication messages per process compared to a single one for $s = 0$ (likewise, $w = 1$ for $s = 1$) for gathering a total of N/n_k elements. Therefore, increasing values of s are expected to negatively impact parallel performance. However, this adversity can be overcome by trading messages for further data movement: firstly, local memory requirements are duplicated to hold two global tensors; secondly, one collective per process is employed to gather all the distributed tensors

consecutively in memory inside the first global (disjoint) buffer; and, lastly, columns are copied in groups to the second buffer in order to compose the global (joint) tensor thereby incurring in the additional movement of N/n_k elements within local memory.

4.2. Distributed-memory higher-order power method

In the next paragraphs we analyse the HOPM in terms of intra-process data movement exclusively. In the particular case of hypersquare tensors ($n_i = n$), a sequential implementation of the HOPM that can be found in Refs. [3, 6] incurs a certain amount of touched memory

$$m_{\text{seq}} = n^d + 2 \sum_{k=2}^{d-1} n^k + (d+3)n, \quad (3)$$

for each one of the aforementioned d external iterations. The first term at the r.h.s. of Eq. (3) corresponds to the size of the input tensor and the second term represents the streamed memory for intermediate tensors. The third term refers to the touched memory of the final output tensor (a vector of size n), all the participating input vectors $(d-1)n$, and the normalization step $3n$. Finally, the total amount of streamed memory of the HOPM algorithm accounted for the d external iterations is simply $M_{\text{seq}} = dm_{\text{seq}}$.

In contrast to Eq. (3), the touched memory expression of the distributed HOPM algorithm loses the symmetry of its sequential counterpart. Each parallel process incurs $M_{\text{par}} = sm_{\text{par},j < s} + m_{\text{par},j = s} + (d-1-s)m_{\text{par},j > s}$, with

$$\begin{aligned} m_{\text{par},j=s} &= \left\lceil \frac{n^d}{p} \right\rceil + 2 \sum_{k=2}^{d-1} \left\lceil \frac{n^k}{p} \right\rceil + 4 \left\lceil \frac{n}{p} \right\rceil + (d-1)n \\ &\approx \frac{m_{\text{seq}}}{p} + \frac{p-1}{p}(d-1)n, \end{aligned} \quad (4)$$

when the external iteration j coincides with the splitting dimension s . Square brackets denote the optimal division but, for the sake of simplicity, we assume a regular division thereby approximating the previous equation so that it can be related to Eq. (3). In fact, the second term of Eq. (4) reveals that the duplication of the input vectors on each MPI process causes a memory overhead over the sequential algorithm. For the remaining $d-1$ external iterations, we get the following expression

$$\begin{aligned} m_{\text{par},j \neq s} &\approx \frac{m_{\text{seq}}}{p} + \frac{p-1}{p} \left(2 \sum_{k=2}^{d-s-l} n^k + (d+2)n \right) \\ &= m_{\text{par},j=s} + \frac{p-1}{p} \left(2 \sum_{k=2}^{d-s-l} n^k + 3n \right), \end{aligned} \quad (5)$$

with $l = 0$ if $j < s$, otherwise $l = 1$ if $j > s$. It can be noticed that Eq. (5) incurs further overhead over Eq. (4) because, contrary to the previous case, now the contraction mode and the splitting index will coincide ($k = s$) during one of the $d-1$ inner TVCs thus yielding larger partial

subtensors as discussed in Section 4.1. This is indeed a very interesting aspect of the dHOPM algorithm: it will lead to $d-1$ underperforming contractions. The final expression for the dHOPM touched memory per process can be written as

$$\begin{aligned} M_{\text{par}} &\approx \overbrace{\frac{M_{\text{seq}}}{p} + \frac{p-1}{p}(d-1)(d+3)n}^{M_{\text{par},\text{min}}} \\ &\quad + \frac{p-1}{p} \left(s \sum_{k=2}^{d-s} 2n^k + (d-s-1) \sum_{k=2}^{d-s-1} 2n^k \right), \end{aligned} \quad (6)$$

which reveals that there is a constant, minimum amount of streamed memory $M_{\text{par},\text{min}}$ caused by the duplicates of the input vectors and the subpar contractions of Eq. (5). On the other hand, the last term of Eq. (6) is highest for $s = 0$ and cancels out for $s = d-1$. It is easy to derive a recursive form

$$\begin{aligned} M_{\text{par},s-1} &= M_{\text{par},s} \\ &\quad + \frac{p-1}{p} \left((d-s-1)2n^{d-s} + (s-1)2n^{d-s+1} \right), \end{aligned} \quad (7)$$

that elucidates a linear increase of data movement with the number of processes and a more complex, nonlinear relationship with the splitting dimension. Contrary to the dTVC algorithm and its later assembly process described at the end of Section 4.1, for the dHOPM one should avoid splitting tensors along their first dimensions, especially when using many processes. This will significantly reduce the movement of data and yield faster computations.

Let us consider the following nondimensional variables: $\hat{p} = p/n$, $\hat{s} = s/(d-1)$, and $\eta^{-1}(\hat{p}, \hat{s}) = pM_{\text{par}}/M_{\text{seq}}$. Figure 2(a) shows the memory ratio η^{-1} of the classical dHOPM for the third- and tenth-order hypersquare tensors considered in this work (see Table 1). In both cases, the data movement more than doubles for $\hat{s} = 0$ and $\hat{p} = 1$. With $d = 3$ the memory ratio increases steadily for decreasing values of \hat{s} while, for $d = 10$, memory effects are limited to a narrow region of low values of \hat{s} . As expected, the touched memory tends to augment with the number of processes and, in any case, if the tensor is split along its last dimension, then $M_{\text{par}} \approx M_{\text{par},\text{min}} \approx M_{\text{seq}}/p$. A similar trend is observed for the other tensors of Table 1 which are not shown in Fig. 2(a) for the sake of conciseness. The only exception to this rule comes from the second-order tensor (matrix) where $M_{\text{par},\text{min}}$ only varies with p , as it can be deduced from Eq. (6), and its value can be significantly larger than those associated with higher-order tensors. Finally, it is worth noting that the expressions (3)–(7) and Fig. 2 are still representative of nonhypersquare tensors provided that the size assigned to each dimension remains about the same order of magnitude.

The classical dHOPM analyzed above can be further optimized for distributed systems as shown in Algorithm 1.

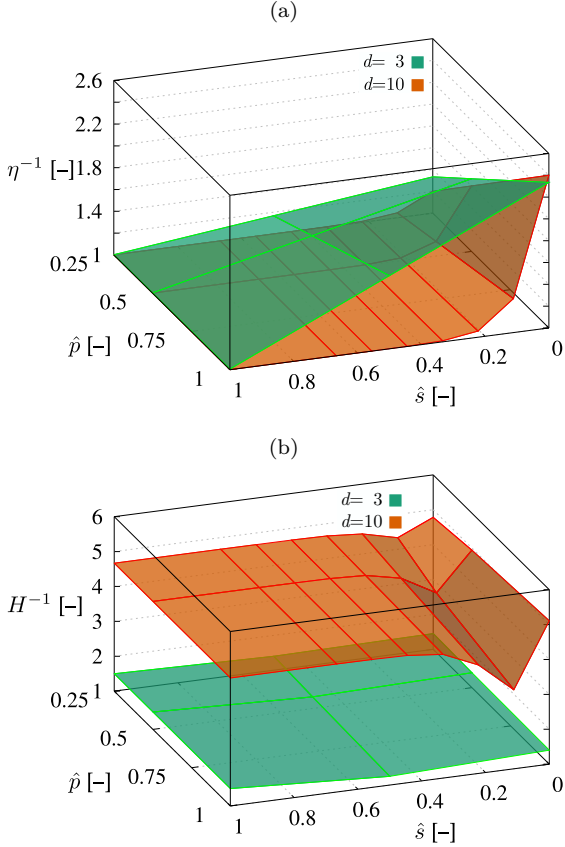


Figure 2: (a) memory ratio (η^{-1}) incurred by the classical, dHOPM implementation and (b) memory ratio (H^{-1}) between this canonical version and dHOPM₃ as a function of the nondimensional number of processes (\hat{p}) and the nondimensional splitting dimension (\hat{s}). Results correspond to the third- and tenth-order tensors of Table 1.

This novel approach, which makes use of three buffers (dHOPM₃), employs two of them \mathcal{Y}_{k-1} and \mathcal{Y}_k to save intermediate tensors and a third one \mathcal{W} to hold previously computed data in memory ($k = \lambda$ or $k = \mu - 1$, see lines 7 or 9) for the next iteration when $j \geq 2$ (line 9). This allows us to save a total of $(d-1)(d-2)/2$ contractions and, as the order of the original input tensor keeps increasing, dHOPM₃ can save up to half of the total contractions required by a canonical, two-buffer algorithm such as the one from Pawłowski et al. [6]. What is more important, the skipped contractions are precisely the most computationally expensive ones since they are carried out on the largest input tensors, which results in even better computational speedups. Another aspect of Algorithm 1 worth mentioning is that it inherently exploits the distributive property of consecutive TVCs and, consequently, the summation required by Eq. (2) when $k = s$ (which implies $j \neq s$) is delayed until the normalization step, thereby reducing the communication to only n_j elements per process at line 14; in other words, the consecutive TVC operations at lines 6–12 are done exclusively on partial, distributed subtensors without incurring in global assembly penalizations. Alternatively, the case $j = s$ implies the disjoint union of \mathbf{x}_j (line

Algorithm 1: Distributed-memory, three-buffer higher-order power method algorithm (dHOPM₃).

Input : distributed d -order tensor $\mathcal{A}^{(p)}$.
Input/Output : d global vectors $\mathbf{x}_0, \mathbf{x}_1, \dots, \mathbf{x}_{d-1}$.
Buffers : inputs $\mathcal{Y}_{k-1}^{(p)}, \mathcal{W}_{j-1}^{(p)}$; output $\mathcal{Y}_k^{(p)}$.

```

1 for  $i \leftarrow 0, 1, \dots$  do
2   for  $j \leftarrow 0$  to  $d-1$  do // Ext. iteration
3      $\lambda \leftarrow 0$  if  $j > 0$ , else  $\lambda \leftarrow 1$ ;
4      $\mu \leftarrow \max(\lambda, j)$ ;
5      $\nu \leftarrow d-1$  if  $j < d-1$ , else  $\nu \leftarrow d-2$ ;
6     if  $j < 2$  then // TVC(1/3)
7        $\mathcal{Y}_\lambda^{(p)} := \mathcal{W}_j^{(p)} \leftarrow \mathcal{A}^{(p)} \times_\lambda \mathbf{x}_\lambda$ ;
8     else
9        $\mathcal{Y}_{\mu-1}^{(p)} := \mathcal{W}_j^{(p)} \leftarrow \mathcal{W}_{j-1}^{(p)} \times_{\mu-1} \mathbf{x}_{\mu-1}$ ;
10     $\mathcal{Y}_{\mu+1}^{(p)} \leftarrow \mathcal{Y}_{\mu+\lambda-1}^{(p)} \times_{\mu+1} \mathbf{x}_{\mu+1}$ ; // TVC(2/3)
11    for  $k \leftarrow \mu+2$  to  $\nu$  do // TVC(3/3)
12       $\mathcal{Y}_k^{(p)} \leftarrow \mathcal{Y}_{k-1}^{(p)} \times_k \mathbf{x}_k$ ;
13    if  $j \neq s$  then
14       $\mathbf{x}_j \leftarrow \sum_p \mathcal{Y}_\nu^{(p)}$ ; // Array reduction
15    else
16       $\mathbf{x}_j \leftarrow \bigsqcup_p \mathcal{Y}_\nu^{(p)}$ ; // Array gather
17     $\mathbf{x}_j \leftarrow \mathbf{x}_j / \|\mathbf{x}_j\|$ ;

```

16) where each process exchanges their calculated portion $\mathbf{x}_j^{(p)}$ for an aggregated communication of n_j elements per process. Finally, the resulting vector is normalized locally by each process at line 17.

Now we can define $H^{-1}(\hat{p}, \hat{s})$ as the streamed memory ratio between the classical dHOPM and our optimal implementation dHOPM₃. Figure 2(b) shows the evolution of H^{-1} for the previously analyzed third- and tenth-order tensors. We obtain two approximately flat surfaces, especially for the low-order tensor, which indicates that this ratio is almost independent of \hat{p} and \hat{s} . Our optimized algorithm economizes about $1.5\times$ of the touched memory for $d=3$ and roughly a fivefold for $d=10$ (with the presence of a minimum of about $3.3\times$). All things considered, Figs. 2(a)–(b) demonstrate that dHOPM₃ can save up to one order of magnitude of streamed memory for higher-order tensors in comparison to a canonical HOPM implementation with naively split tensors.

As previously mentioned, Eqs. (4)–(7) do not account for inter-process data movement. On the one hand, for all the external iterations except one, the resulting vector \mathbf{x}_j must be entirely reduced by all processes (see line 14 of Algorithm 1), otherwise only a portion of this array is gathered (line 16). The actual amount of data being both transferred and computed ultimately depends on the algorithm employed underneath the functions `MPI_Allgather` and `MPI_Allreduce` and it is likely to change at runtime based on the message size, the number of processes and the network topology [29]. For example, the straightforward

ward ring algorithm, which is bandwidth-optimal, suitable for large messages, and works with any value of p , yields $4n(p-1)/p$ extra touched memory per process, a quantity that can be appended to the term $M_{\text{par},\text{min}}$ in Eq. (6). It can be easily inferred that the inter-process contribution reaches its maximum for $d=2$ and $\hat{p}=p/n=1$, increasing the value of $M_{\text{par},\text{min}}$ by up to $4/7 \approx 57\%$. In the case of hypersquare tensors, this constant number remains independent of the splitting dimension and can be halved by storing separate copies of the input tensor \mathcal{A} with different splittings in order to foster partial gatherings of \mathbf{x}_j .

4.3. Task-based parallelization of the dHOPM₃ algorithm

We take the opportunity to describe herein the shared-memory parallel strategy adopted for dHOPM₃ in which every contraction (lines 7, 9, 10, and 12 of Algorithm 1) takes advantage of task-based parallelization. In contrast to ubiquitous OpenMP parallel for loops, tasks permit to overlap computations corresponding to different TVC instances, thereby maximizing the parallel performance over fork-join. This key novel parallel design is exemplified below for a single TVC operation, defined by the `getvc` function [10], which is split in several tasks:

```

if (trans == iZero) { // Matrix-vector (row-major)
    ...
    for (intT i = iZero; i < m; i += bsM) {
        ...
        #pragma omp task depend(in : x[iZero: n]) \
            depend(in : a[i*lda:bsMA*n]) \
            depend(out: y[i :bsMA ])
        getvc(layout, trans, bsMA, n,
            alpha, a + i*lda, lda,
            x, incx, y, beta, y + i, incy);
    }
} else { // Vector-matrix (row-major)
    ...
    for (intT j = iZero; j < n; j += bsN) {
        ...
        #pragma omp task depend(in : x[iZero:m ]) \
            depend(in : a[startl:size]) \
            depend(out: y[j :bsNA])
        getvc(layout, trans, m, bsNA,
            alpha, a + startl, lda,
            x, incx, y, beta, y + j, incy);
    }
}

```

Each TVC is assigned a certain number of tasks (i.e., granularity) inside a loop that can be executed concurrently. We establish task data dependencies via `depend` clauses for the input vector \mathbf{x} and tensor \mathbf{a} as well as the output tensor \mathbf{y} to ensure the correct order of execution of different TVCs and normalization steps as indicated in Algorithm 1. The task granularity is such that there are more tasks than threads, which permits the overlapping of subsequent TVC operations. This is clearly seen in Fig. 3, which corresponds to a real execution carried out on MN4, instrumented with Extrae and visualized with Paraver² for a tenth-order

tensor distributed among four processes. While Fig. 3(a) covers a full dHOPM₃ execution ($i=0$), the figure below is a zoomed version towards the end of the first external iteration $j=0$. In both figures, subsequent TVC operations are represented with rectangles (tasks) of different colors. As previously mentioned, threads can start executing blocks of different colors as quickly as possible. There are still some relatively small white gaps that evidence code sections with no CPU usage and correspond exclusively to the final normalization phase (lines 13–16 of Algorithm 1) where synchronous collective communication takes place and MPI processes must wait for the slowest one due to system imbalance. Both subfigures also reveal how computational costs greatly reduce after each contraction as the resulting tensor loses one dimension and its size decreases by about one order of magnitude.

Contrary to tasks, a shared-memory strategy based upon the fork-join paradigm (see the code snippet from Ref. [8]) and, by extension a CUDA-based implementation, presents one implicit synchronization per contraction. Consequently, a Paraver trace of such parallel execution (not shown here for the sake of conciseness) would have shown white gaps towards the end of each TVC where idle threads must wait to the slowest one to finish its corresponding computation, close the parallelism (join) and, finally, reopen it for the next contraction (fork). All these additional periods of CPU inactivity increment the computational time and the application imbalance that ultimately result in an overall lower speedup with respect to the task-based implementation.

5. Performance evaluation

This section evaluates the performance of the distributed TVC and HOPM algorithms detailed in previous sections of this manuscript after describing the numerical environment setup. The complete source code of our dTVC library is made publicly available under the GPLv3 license in Ref. [10].

5.1. HPC systems and code setup

We have targeted three different hardware architectures available at the Barcelona Supercomputing Center (BSC). The first one is the general-purpose MareNostrum 4 (MN4) supercomputer, whose compute nodes are composed of two Intel Xeon Platinum 8160 CPUs with 24 cores each (hyperthreading disabled), 33 MiB of L3 cache, and AVX-512 SIMD instructions. The system memory is based on DDR4 and peaks at a theoretical bandwidth of 128 GB/s per socket (256 GB/s per node). The second architecture is the CTE-ARM cluster where each compute node integrates four Fujitsu ARM A64FX CPUs with 12 cores, a last level cache of 8 MiB, and 512-bit SVE instructions. Each socket has 8 GiB of installed HBM2 reaching theoretically 256 GB/s (1024 GB/s per node). Lastly, the third architecture is the CTE-POWER cluster equipped with four NVIDIA Volta

²Extrae and Paraver are available at: <https://tools.bsc.es/>

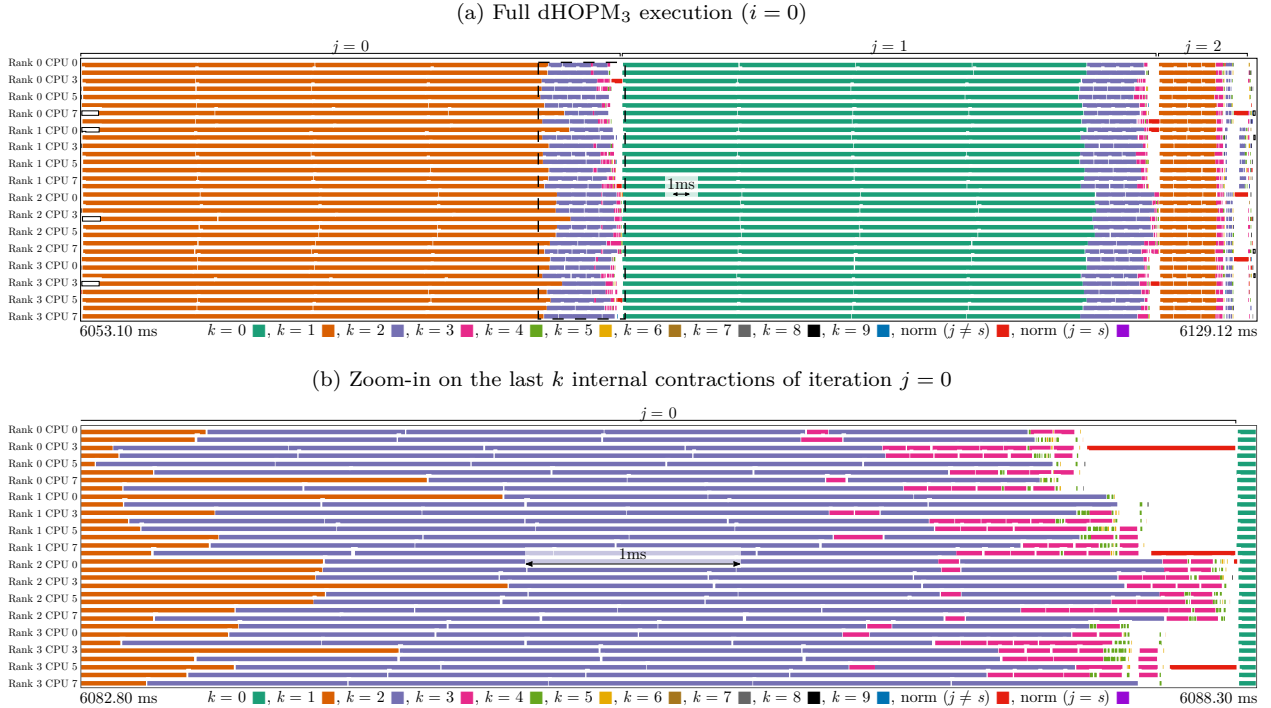


Figure 3: Paraver traces from the hybrid execution of (a) the dHOPM₃ algorithm and (b) a zoom-in view of the last k internal contractions of iteration $j = 0$ using the tenth-order tensor of Table 1 split along its last dimension. Traces obtained on MN4 using 4 MPI processes, 8 cores per process, and 32 OmpSs-2 tasks per process for illustration purposes.

V100 GPUs per compute node. Each graphic card features 16 GiB of HBM2 reaching a theoretical peak bandwidth of 900 GB/s (3600 GB/s per node).

Table 1: Number of 8-byte floating-point elements and corresponding memory footprint (measured in GB) for the hypersquare tensors used in this work.

Order	Elements	Memory
2	30623^2	7.50
3	979^3	7.51
4	175^4	7.50
5	63^5	7.94
6	31^6	7.10
7	19^7	7.15
8	13^8	6.53
9	10^9	8.00
10	8^{10}	8.59
Avg.	9.4×10^9	7.54

The tensors used in this work are listed in Table 1. We choose hypersquare and up to tenth-order dense tensors. In principle, they are filled with 8-byte floating-point numbers (i.e., doubles) following other works [6, 8]. Lower-precision floats will be introduced later in Section 5.5. When possible, each tensor dimension size has been intentionally chosen to prevent it from being a multiple of the vector length—which is 8 when using doubles and the 512-bit SIMD/SVE instruction set—with the aim of fostering scenarios showcasing unaligned memory accesses as well as

peeling and remainder loops. The aforementioned tensors average 7.5 GB of memory in order to guarantee that TVC operations are limited by the system memory bandwidth while fitting within the rather small HBM2 memory incorporated in two of the three systems described above. Consequently, larger tensors with vector-friendly dimension sizes are expected to yield better performance figures.

With regard to code compilation, we utilize the LLVM infrastructure unless otherwise stated. In particular, we employ the Clang++ 16.0 compiler that supports both the OpenMP [30] and OmpSs-2 [31] programming languages allowing for data-flow parallelization via task annotations. In order to obtain the maximum performance, we use the flag `-march= native` to enable CPU specific optimizations. The combination of flags `-Ofast` and `-mprefer-vector-width=512` are used to exploit 512-bit vector instructions. In addition to this, the flag `-fopenmp` enables OpenMP pragma directives used for both vectorization and parallelization of the code: unless otherwise stated, shared-memory parallelization is achieved via fork-join, “parallel for” loops. Furthermore, the flag `-f1to` enables interprocedural (i.e., link-time) optimizations. Other code parameters are the alignment of buffers to transparent huge pages of 2 MiB and the loop unrolling factor set to 8. For GPU devices, we make use of the latest cuBLAS 10.2 library officially supported by the architecture vendor.

Each benchmark steadily executes a particular TVC or HOPM computation during five seconds allowing tens or even hundreds of kernel calls to retrieve statistical figures.

Strong scalability tests are conducted on up to 128 MPI processes which are bound to distinct NUMA nodes or GPU devices to allow for hybrid or heterogeneous parallelization, respectively. We employ the MPI libraries provided by the hardware manufacturers: Intel MPI on MN4, Fujitsu MPI on CTE-ARM and IBM Spectrum on CTE-POWER. Besides, we choose NVIDIA NCCL over CUDA-aware MPI functions for best performance. We employ three performance metrics: (i) the normalized bandwidth that is obtained after dividing by the theoretical peak bandwidth corresponding to each architecture, (ii) the kernel throughput measured in iterations per second (it/s) and (iii) the normalized kernel throughput measured in iterations per second per MPI process (it/sp). We remind the reader that the memory bandwidth is the touched (i.e., streamed) memory per unit of time and the STREAM benchmark [32], particularly the `triad` function, reports the following figures on each NUMA node or GPU device: 104.5 GB/s (81.6% of the theoretical peak) on MN4, 153.7 GB/s (60%) on CTE-ARM, and 556.2 GB/s (61.8%) on CTE-POWER.

5.2. State-of-the-art performance of the tensor–vector contraction

We find it convenient to give the reader a notion about the expected parallel performance of the dTVC algorithm using the software available in the literature. To this end, we provide a comparison of our proposed solution against the massively parallel tensor contraction (CTF) framework [23] (Deinsum [25] does not currently support tensor–vector contractions). This framework enables hybrid parallelism via MPI and MKL libraries and also makes extensive use of the optimized kernels provided by the later, namely: BLAS, LAPACK, and ScaLAPACK. We compiled CTF against the latest Intel software suite available on MN4 (Intel oneAPI 2022.3) and the recommended high performance tensor transpose (HPPT) library for maximum performance. CTF can be regarded as a DSL for tensor algebra that allows, for instance, to effortlessly express a 2-mode tensor–vector contraction (i.e., $\mathcal{Y} = \mathcal{A} \times_2 \mathbf{x}$) within a single line of C++ code:

```
Y["ijl"] = A["ijkl"]*x["k"];
```

assuming that \mathcal{A} (i.e., `A["ijkl"]`) is a fourth-order tensor. There are two important aspects about the previous line of code that are worth discussing. Firstly, both tensors and the vector are implicitly distributed among different MPI processes and, therefore, this operation is not exposed to the user (CTF claims to minimize communication costs). Secondly, each tensor operation such as the one indicated above is susceptible³ to assemble the resulting partial subtensors $\mathcal{Y}^{(p)}$, in order to form the global tensor \mathcal{Y} (i.e., `Y["ijl"]`). Therefore, benchmarking such a CTF code example is similar to timing the distributed contraction in addition to the tensor assembly. This global gathering

³This will depend on the contraction mode, the tensor splitting assumed by CTF, and the number of MPI processes.

incurs MPI communication, which can consume more computational time than the tensor contraction itself. This is undesirable, especially in the case of the dHOPM₃, where the partial subtensors resulting from each dTVC operation do remain distributed throughout the entire execution (see Algorithm 1).

Figure 4 presents a strong scalability performance comparison between our proposed dTVC algorithm and the CTF implementation using up to 8 MPI processes (4 compute nodes) on MN4. We show the normalized throughput measured in it/sp because, contrarily to CTF, our implementation seeks one-dimensional optimal splittings (see Fig. 1). Consequently, order 7–8 tensors are contracted with 7 processes, while the ninth-order tensor only exploits 5 processes. Next, for each tensor in Fig. 4, the corresponding results are the aftermath of averaging the normalized throughput values over all contraction modes and all splitting dimensions (d^2 times) in the case of our implementation. Since CTF splits the tensors internally, the associated results are only averaged over d contraction modes. In both cases, the overhead related to the tensor assembly discussed above is accounted for.

We shall start by focusing on the results of Fig. 4 corresponding to a single MPI process ($p = 1$), where only shared-memory parallelism is available and there is no need to form a global output tensor. In this situation, our distributed implementation is able to sustain more than 8 it/sp across all tensors. On the other hand, CTF only remains competitive for the matrix case (order 2) and gradually loses performance, being more than four times slower for the tenth-order tensor due to the subpar performance of MKL’s batch-strided kernels employed for the internal contraction modes [8]. Getting back to the matrix case using our proposed implementation (solid bars), it can be readily seen that increasing the number of distributed processes has no visible impact on performance: indeed, the corresponding results are all above 80% of the theoretical peak performance of the machine. This is expected because the amount of memory being communicated using one-dimensional splitting is reduced by a factor of $30623\times$ with respect to the input tensor size (7.5 GB). In contrast, much smaller factors are associated with higher-order tensors (e.g., $8\times$ for the tenth-order tensor) and thus larger communication overheads as it can be inferred from the remaining solid bars of Fig. 4. In this regard, CTF presents a rather strange behaviour for third- and especially second-order input tensors with throughput values well below 0.5 it/sp, thereby making it unsuitable for distributed matrix–vector (or vector–matrix) multiplication of large square matrices. On the other hand, CTF starts approaching and can even surpass the performance of our implementation for higher-order tensors and more than four MPI processes. But such cases are largely dominated by the time spent assembling the global output tensor, which can be more than one order of magnitude higher than that of the TVC operation itself. Indeed, the bandwidth associated with $d > 6$ and $p = 8$ do not attain 10% of the peak perfor-

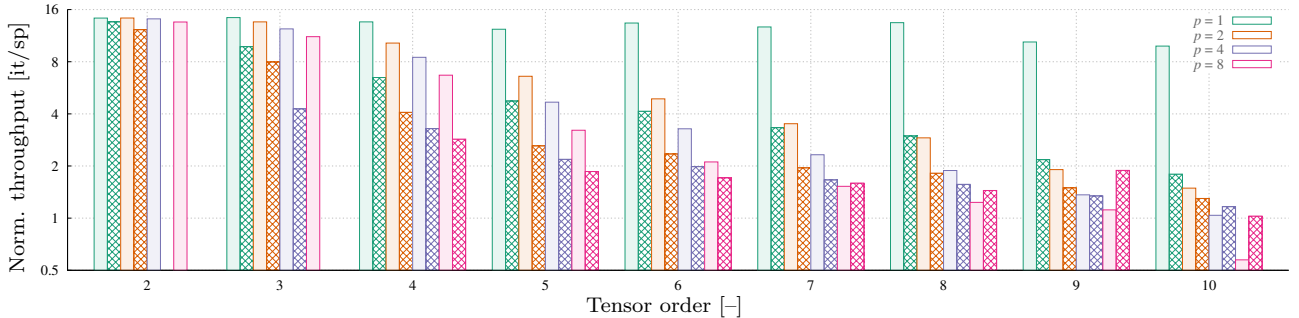


Figure 4: dTVC normalized throughput (including global assembly of the output tensor) measured as the number of iterations per second per MPI process (it/sp) over all contraction modes and all splitting dimensions for the tensors of Table 1. Strong scalability results using up to 8 MPI processes on MN4 employing our proposed distributed TVC algorithm (solid fill) and the CTF implementation (pattern fill).

mance and hence cannot be considered representative of HPC scenarios. Finally, it is worth mentioning that we have not optimized neither the disjoint union, Eq. (1), nor the global reduction, Eq. (2), operations involved in the formation of the global output tensor.

Figure 4 emphasises the criticality of the distributed tensor–vector contraction and, particularly, its associated global reconstruction process. In this sense, the convenience of expressing tensor contractions straightforwardly through a DSL (via CTF, tiledArray, and similar libraries), can be counterbalanced by the lack of performance arising from the continuous assembly of the distributed output subtensors. In the remainder of this work, we will evaluate the performance of the dTVC algorithm without reconstruction. As previously discussed, this operation is irrelevant in the dHOPM₃ because it naturally exploits the distributive property of the tensor contraction.

5.3. Distributed native tensor–vector contraction performance

Table 2 reports on the results of the dTVC ignoring the global construction of the final tensor, which allow us to focus exclusively on the computational kernel performance. In particular, we are concerned about the matricized tensor’s shape —tall and skinny vs. short and fat matrices— on the contraction performance. In addition to this, we propose the comparison of the looped approach based on state-of-the-art MKL kernels against our CPU-native implementation using two compilers: icpx (Intel) and clang++ (LLVM). We remind the reader that results are averaged over all contraction modes and all splitting dimensions and normalized by the theoretical peak bandwidth corresponding to eight MPI processes on MN4 (order 7–9 tensors exploit lower MPI processes due to the one-dimensional optimal splitting, as previously discussed).

It can be readily seen on Table 2 that the looped dTVC algorithm based on MKL’s batch-strided kernel yields the worst results, with relatively low average bandwidth and high standard deviation rates. The high variability of the results, except in the matrix case, evidence the lack of mode-oblivious properties of this implementation despite the fact that it is based upon a carefully optimized kernel.

As demonstrated in Ref. [6], MKL is more sensitive to the shape of the matricized tensor and, in the case of concatenated small MVMs, LIBXSMM may be able to report slightly better figures. In any case, they are not expected to remain competitive against those shown in the next two columns, which belong to our CPU-native dTVC implementation using the same compilation stack as well as the LLVM infrastructure. Differences between compilers are minimum and, in both cases, our proposed algorithm achieves almost three quarters of the theoretical peak performance (1024 GB/s) with a standard deviation below 10%. We remind that this low value accounts for changes not only in the contraction mode, but also in the splitting dimension which ultimately affects the shape of the matricized form of the tensors. Therefore, we can affirm that the distributed strategy proposed in this work remains oblivious to these two variables.

Table 2: dTVC normalized, averaged bandwidth (measured as a percentage of the theoretical peak value) and corresponding unbiased, sample standard deviation percentage (within brackets) over all contraction modes and all splitting dimensions for the tensors of Table 1. Results correspond to 8 MPI processes on MN4 and two TVC algorithms (looped and native).

Order	Looped (MKL)	Native (icpx)	Native (clang++)
2	76.4 (10.7)	77.5 (15.6)	80.7 (6.5)
3	65.7 (41.5)	82.6 (1.9)	83.1 (1.8)
4	58.3 (52.2)	80.4 (5.7)	81.1 (5.9)
5	52.8 (57.3)	76.9 (6.3)	77.6 (6.3)
6	47.0 (61.6)	72.7 (8.3)	73.3 (8.6)
7	39.7 (66.4)	66.2 (9.2)	66.6 (9.5)
8	38.8 (67.5)	66.3 (9.0)	66.8 (8.7)
9	40.7 (67.8)	69.8 (9.2)	70.1 (9.7)
10	38.5 (70.2)	70.6 (8.4)	70.9 (9.3)
Avg.	50.9 (55.0)	73.7 (8.2)	74.5 (7.4)

Figure 5(a) shows that, in general, the averaged bandwidth of all tensor contractions is between 70% to 85% of the theoretical peak on MN4, which is in good agreement with the STREAM benchmark on a single NUMA node of this architecture (81.6%). This rather small performance variability of about 15% is inevitable: for instance, not

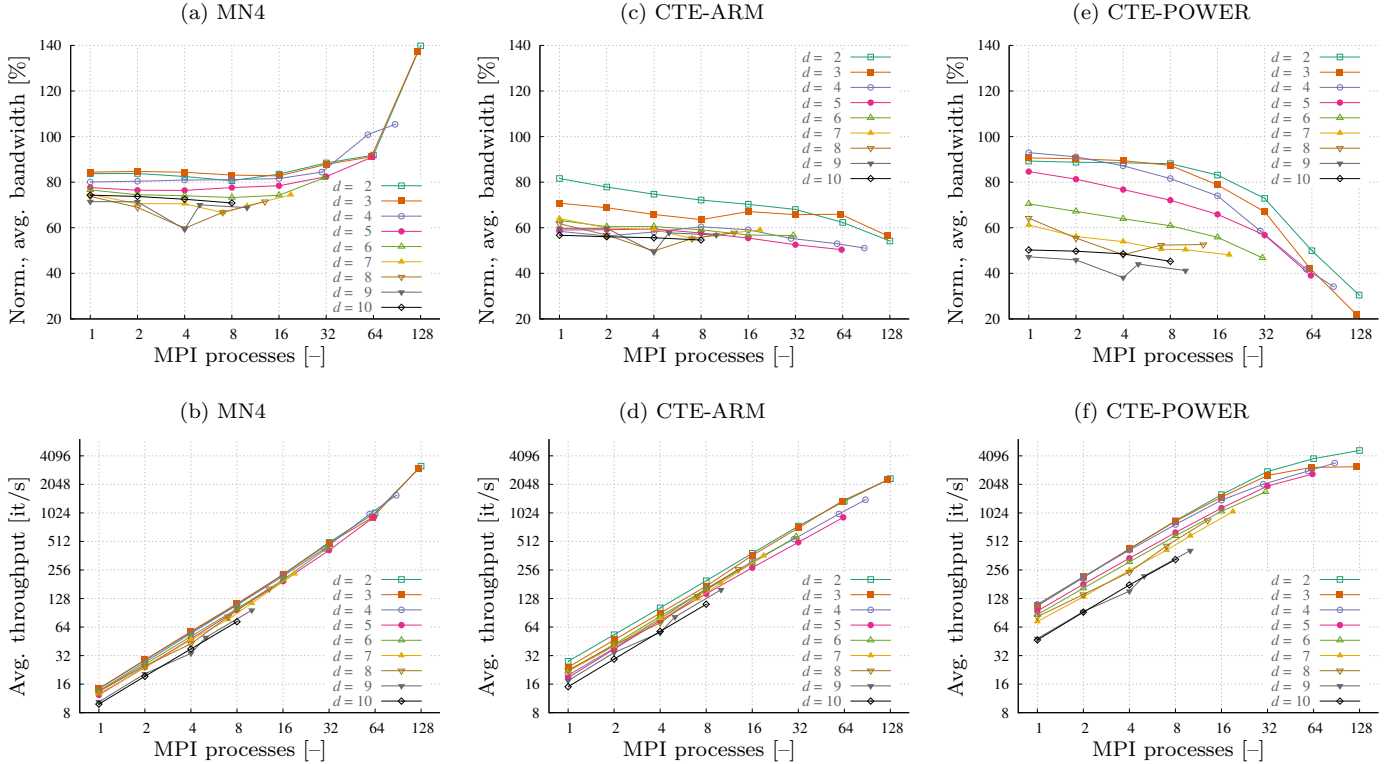


Figure 5: dTVC normalized, averaged bandwidth and averaged throughput over all contraction modes and all splitting dimensions for the tensors of Table 1. Strong scalability results using up to 128 MPI processes on (a)–(b) MN4, (c)–(d) CTE-ARM, and (e)–(f) CTE-POWER.

all the tensors have the exact same memory footprint as reported in Table 1. With more than 16 MPI processes, the strong scalability performance begins to increase slightly as the bandwidth bottleneck moves from main memory to L3 cache. Figure 5(b) shows absolute dTVC performance values in the form of an averaged throughput measured in kernel invocations per second (it/s). We can see how the curves associated with each tensor are very close to each other except for $d = 9, 10$ due to their larger memory footprint (in relative terms: 6.7% and 22.7%, respectively). Note also that these two higher-order tensors cannot be computed with more than 10 and 8 MPI processes, respectively, when using one-dimensional splitting. We confirm the linear (and superlinear) scalability already predicted by the bandwidth curves. In the light of the results gathered in Figs. 5(a)–(b), it is the first time that a distributed tensor–vector contraction remains oblivious to MPI splitting, contraction mode, and also tensor order, provided that the tensor size does not vary significantly.

Figures 5(c)–(f) report on the dTVC performance for the CTE-ARM and CTE-POWER systems, respectively. We use the CPU-native, TVC algorithm to benchmark the ARM architecture while GPUs are evaluated against a looped TVC implementation making use of cuBLAS. Starting with the CPU case, Fig. 5(c) shows slightly decreasing values of the normalized bandwidth, especially for $d > 3$, but they are overall within the range of 50% to 70% of the theoretical peak (on average, STREAM reports 60%

on a single node). The almost linear throughput curves of Fig. 5(d) are a bit more spread than those of MN4 but, once more, we can say that our novel implementation remains oblivious to splitting, contraction mode and tensor order for this particular architecture. Finally, note that although CTE-ARM starts with better absolute throughput values over MN4 thanks to its high-end memory, its overall worse strong scalability yields subpar performance with 128 MPI processes.

Figure 5(e) shows the dTVC performance on GPUs using state-of-the-art cuBLAS kernels. We observe a large variability going from 90% of the theoretical bandwidth peak to only 20% (on average, STREAM reports 61.8% on a single graphics card). Interestingly, only the last two higher-order tensors report somewhat constant bandwidth figures, but 10% to 15% below the reference STREAM benchmark value. This is expected since batched kernels do incur some overhead while enqueueing consecutive multiplication kernels within a unique function call. This distributed GPU implementation based on looped TVC lacks the obliviousness of its CPU counterpart implementation. In absolute terms, see Fig. 5(f), the CTE-POWER attains maximum throughput values around 4096 it/s, a quantity that is not much higher than the one reported by a general-purpose architecture endowed with DDR4 memory. It is worth highlighting that dTVC remains an embarrassingly parallel application (the final disjoint union operation is discarded) with zero MPI communication parts and, consequently, the

scalability drop in Fig. 5(f) is likely to be attributed to the rather low device occupancy. This supports our choice of one-dimensional tensor splittings since very fine-grain parallelization tends to hamper performance, especially on this type of accelerators.

5.4. Distributed, native higher-order power method performance

For the sake of conciseness, we only evaluate the performance of the optimized dHOPM₃ (Algorithm 1) and, therefore, naive implementations are discarded in this work. This choice is justified because our results are ultimately compared against theoretical bandwidth values in order to give an accurate representation on how our distributed algorithm truly performs on a given architecture. In addition to this, tensors are split along their last dimension, $\hat{s} = s/(d-1) = 1$, to ensure minimal streamed memory and best throughput (see Fig. 2).

Table 3 confirms the conclusions previously drawn in Section 4.3 by demonstrating how a genuine data-flow execution based on either OpenMP tasks (OMP_{tk}) or OmpSs-2 tasks (OSS_{tk}) can provide, on average, up to a 10% increase in memory bandwidth over a canonical strategy using fork-join, parallel for constructs (OMP_{fj}). OpenMP tasks are slightly faster than OmpSs-2 tasks in this particular case, which can be attributed to the design differences between these two runtimes. It is worth mentioning that these moderate speedups are limited by the synchronous MPI collectives at the end of each external iteration of dHOPM₃. In cases where the HOPM requires many iterations to reach converge ($i \gg 1$), task-based relaxation techniques similar to those that have been put in place in classical linear algebra iterative algorithms [33] could be employed to remove global synchronizations and approximate the base of output vectors. Such a case is beyond the scope of this work, but represents a real scenario where task-based parallelization could yield additional advantages.

Table 3: dHOPM₃ normalized bandwidth (measured as a percentage of the theoretical peak value) over the last splitting dimension for the tensors of Table 1. Results correspond to 8 MPI processes on MN4 and three parallel implementations.

Order	OMP _{fj}	OMP _{tk}	OSS _{tk}
2	66.9	75.1	73.4
3	63.8	83.7	80.0
4	62.3	80.9	77.6
5	59.7	74.1	71.8
6	59.8	67.9	65.8
7	54.2	59.8	58.4
8	51.9	62.0	60.9
9	60.2	63.3	62.9
10	59.6	70.9	69.5
Avg.	59.8	70.8	68.9

Figure 6(a) shows the normalized bandwidth of dHOPM₃ on MN4, which presents similarities with the dTVC bandwidth results previously shown in Fig. 5(a). The variability

range is expected to widen due to the continuous decrease of the tensor size after each contraction but, in general, normalized values are between 60% to 85% most of the time. Contrarily to dTVC, dHOPM₃ is not an embarrassingly parallel application and, sometimes, the cost of synchronous communications can be as important as computations as it is the case with $d = 2$ and $p > 32$. When looking at the absolute throughput, see Fig. 6(b), it starts at about 4–8 it/s and reaches between 512–1024 it/s with 128 MPI processes for $d = 3, 4$ while it drops by a factor of two for the matrix case due to excessive synchronization. It can be readily seen that Figs. 5(b) and 6(b) are reasonably equivalent with the particularity that there exists a factor above two between them. This is because the computational time of dHOPM₃ is primarily dominated by two contractions, i.e. $k = 1$ for $j = 0$ and $k = 0$ for $j = 1$, as illustrated in Fig. 3(a).

Figures 6(c)–(f) show the dHOPM₃ results on the other two architectures equipped with high bandwidth memory. In the case of the CTE-ARM cluster, each contraction makes use of our CPU-native TVC algorithm and no significant differences can be appreciated between Figs. 5(c) and 6(c). Nevertheless, it is true that, in the case of lower-order tensors, dHOPM₃ bandwidth values are more sensible to the number of processes due to synchronous communication. A similar factor above 2× between dTVC and dHOPM₃ throughputs is found on CTE-ARM. Looking at the results obtained on these two CPU-based architectures, it can be inferred that the dHOPM₃ algorithm inherits the obliviousness of the native dTVC kernel it is built upon.

Figure 6(e) shows the dHOPM₃ normalized bandwidth under Volta GPUs. Compared to the dTVC results of Fig. 5(e), dHOPM₃ performance is better in the sense that curves do remain closer to each other, especially with moderate values of p . This is in contrast to what is observed on the two previous architectures. As a reminder, dTVC results were averaged over *all* the splitting dimensions while dHOPM₃ figures are only calculated for the *last* splitting dimension for minimal memory footprint. For this reason, one can expect higher bandwidth values for dHOPM₃ up to a certain number of processes; otherwise, the relatively low GPU occupancy combined with the increasing synchronization costs of collectives results in an important reduction of bandwidth, with values as low as 10% with 128 MPI processes. It is worth noting that these are indeed the best results one can achieve in terms of communication: memory is transferred between devices directly via the NCCL library that provides genuine nonblocking calls to MPI functions from the CPU host. Other communication approaches, not shown here for the sake of brevity, always resulted in subpar performance. Finally, Fig. 6(f) confirms that the maximum throughput achieved on GPUs is above 512 it/s and does not necessarily correspond to the largest number of processes. Considering all the strong scalability results presented in this section, none of the clusters equipped with high bandwidth memory is able to surpass a general purpose supercomputer with regular DDR4 mem-

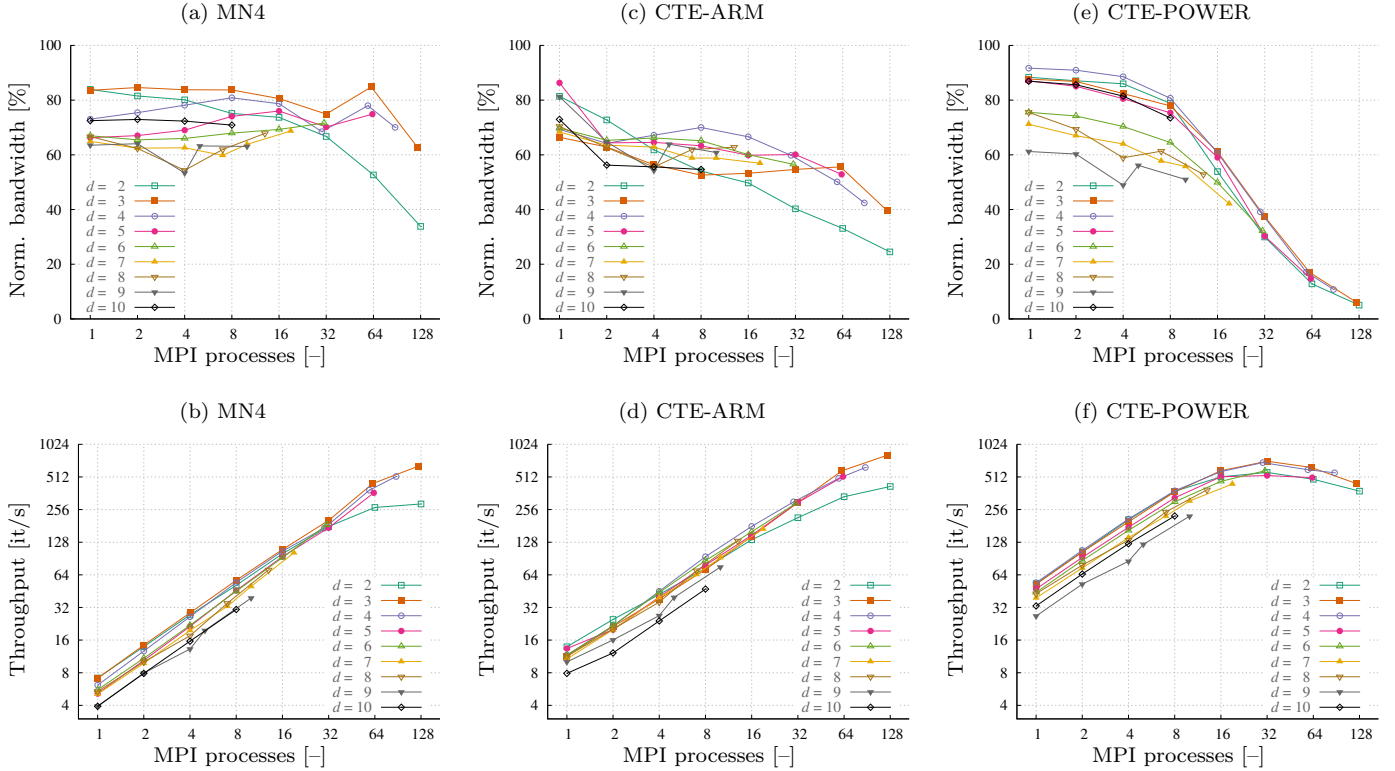


Figure 6: dHOPM₃ normalized bandwidth and throughput for the tensors of Table 1 split along their last dimension. Strong scalability results using up to 128 MPI processes on (a)–(b) MN4, (c)–(d) CTE-ARM, and (e)–(f) CTE-POWER.

ory. This is mainly attributed to the low-capacity HBM2 modules installed on these systems.

5.5. Mixed precision effects on performance

Since both dTVC and dHOPM remain memory bounded algorithms, mixed precision can be employed to further increase their throughput. In fact, mixed precision is a very popular technique actively used in deep learning applications [34, 35]. In this work, low precision is used exclusively as a storage format and we promote numbers to high precision, i.e. by doubling their bit representation, just before computing them. Therefore, every arithmetic operation, besides accumulations, is done in high precision. Calculated quantities are then converted back to their original storage precision. It is worth noting that mixed precision also affects communication and hence requires the development of ad-hoc MPI functions that enable high-precision scalar and array sums while keeping data transfers in low precision.

We consider three mixed precision formats: single-double, half-single, and brain-single. The half format stands for the IEEE 754-2008 binary16 standard while brain consists of a 16-bit truncation of the binary32 type from the same standard. While it is straightforward to create a fast truncation algorithm for brain type conversions, we employ a third-party library [36] for half type conversions on MN4 exclusively because its CPUs do not provide native hardware support. Note also that conversions made

in software with this library inhibit the vectorization of some parts of our TVC library, notably while storing the results from vector-matrix multiplication kernels, vector updates (i.e., `axpy` functions), and global array reductions via MPI. As a result, the entire application performance plummets making it unusable. To mitigate this, we introduce an intermediate array to cache high-precision results. The following code snippet extracted from Ref. [10] and corresponding to the `axpy` function illustrates this:

```
static const intT unrollY = simdObjSz*simdObjSz;
const intT nU = MULTIPLE(n, unrollY);
objT wrk[unrollY] __attribute__((aligned(cacheLn)));

const lobjT * __restrict__ p_x = x;
const lobjT * __restrict__ p_y = y;
for (intT ui = iZero; ui != nU; ui += unrollY) {
    #pragma omp simd simdlen(simdObjSz)
    for (intT ri = iZero; ri != unrollY; ++ri) {
        wrk[ri] = a*OBJT(p_x[ri]) + b*OBJT(p_y[ri]);
    }
    for (intT ri = iZero; ri != unrollY; ++ri) {
        p_y[ri] = LOBJT(wrk[ri]);
    }
    p_x += unrollY; p_y += unrollY;
}
```

Caching is achieved by the array `wrk` that is aligned to a cache line and can have an arbitrary size multiple of the SIMD vector length known at compile time. It

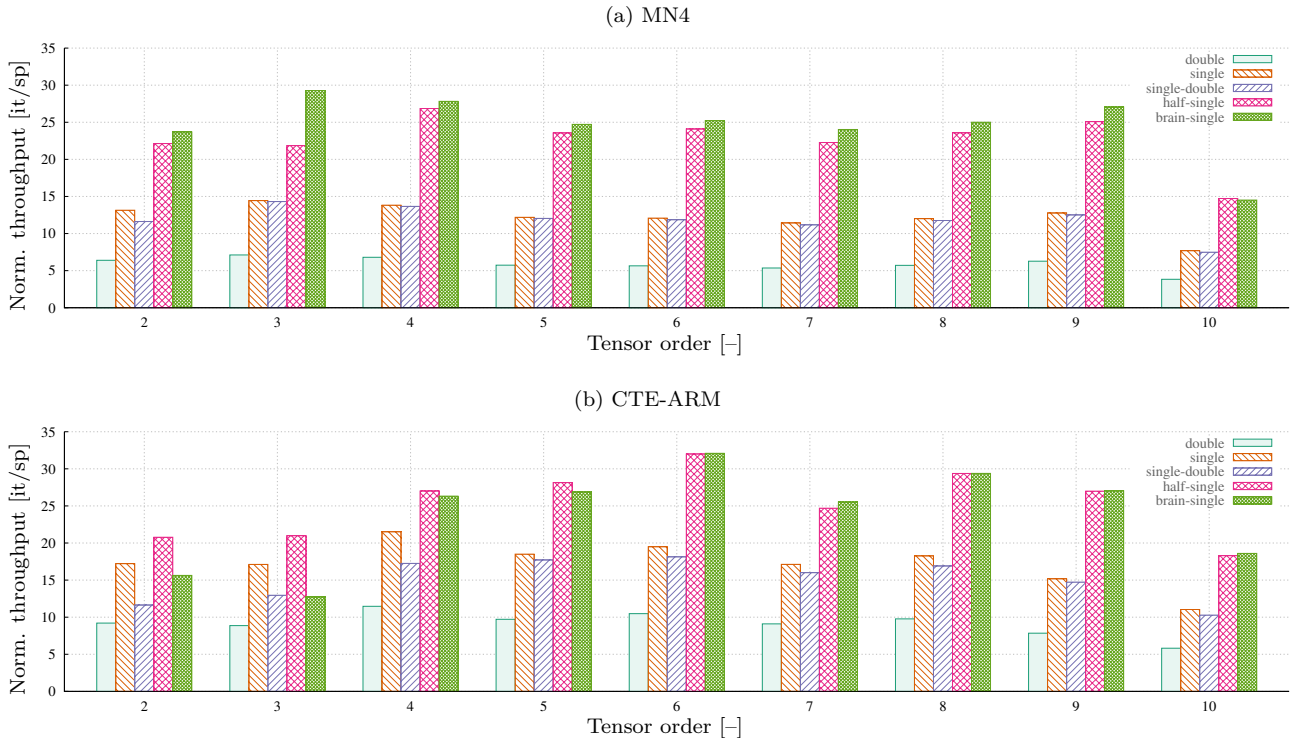


Figure 7: dHOPM₃ normalized throughput for the tensors of Table 1 stored in different floating-point precision formats and split along their last dimension. Results correspond to 8 MPI processes on (a) MN4 and (b) CTE-ARM.

can be readily seen that the main loop is divided into one outer loop and two inner loops (the remainder loop is omitted for simplicity). The first inner loop can be vectorized via OpenMP pragmas and accomplishes the actual computation, $\alpha\mathbf{x} + \beta\mathbf{y}$, after promoting both input arrays to higher precision (O_BJT). The second inner loop cannot be vectorized due to the type conversion to low precision (L_OB_JT) but the compiler is able to automatically unroll it thereby achieving a throughput comparable to its single precision, fully vectorized counterpart.

Figure 7 shows the absolute performance of the dHOPM₃ algorithm for various floating-point precision formats on two CPU architectures and eight processes. Starting with MN4, the throughput values corresponding to double precision are taken directly from Fig. 5(b). With single and single-double precision the throughput is practically increased by a factor of two regardless of the tensor order. Brain-single precision doubles the speed of single precision, yielding about 4× speedup with respect to double precision. The half-single precision results obtained with the half library are quite competitive with the previous case demonstrating the advantages of caching. Interestingly, there is a considerable performance hit of −34% for $d = 3$, which makes for an effective speedup of 3.1× over double precision. In general, the matrix case ($d = 2$) yields slightly worse results for half-single and brain-single precision, which is attributed to the global array reduction involving tens of thousands of elements per process, all carried out in mixed precision arithmetic. By contrast,

mixed precision dTVC does not exhibit such behaviour since it does not rely on collectives. Generally, dTVC and dHOPM₃ mixed precision results show similar trends, but the latter constitutes a more challenging example due to its variety of kernels and synchronous collectives.

Figure 7(b) shows inconclusive results on the ARM architecture. On the one hand, using single precision does not necessarily double the performance as it was the case of MN4. On the other hand, and contrarily to what is observed in MN4, the single-double results show hindered performance for lower-order tensors ($d < 4$). Although the CPUs of CTE-ARM provide hardware support for half precision floating points, half-single results reflect a speedup below 2× w.r.t. single precision and about 3× w.r.t. double precision. Similarly to MN4, worse mixed precision speedup figures are associated with lower-order tensors due to the increasing cost of mixed precision collectives. Finally, the brain-single results based upon a simple truncation made in software show a performance similar to half-single mixed precision arithmetic for most tensors ($d > 3$).

Finally, we do not have mixed precision results on GPUs since, to the best of our knowledge, NCCL does not provide mixed precision MPI routines. Moreover, CUDA kernels do not offer the degree of flexibility required to consistently integrate all the mixed precision kernels needed by the distributed higher-order power method. In this regard, further work is needed to extend the support for mixed precision in HPC software, including message-passing interface (MPI) libraries.

6. Conclusions and future work

This work has presented a distributed tensor–vector contraction algorithm built on top of a CPU-native TVC shared-memory library recently published. It has also introduced a carefully optimized, distributed higher-order power method, dHOPM₃, which takes advantage of data-flow parallelization. The performance of dTVC is compromised when the splitting and contraction modes coincide and, while this can be easily circumvented for one dTVC over a particular contraction mode, it is unavoidable in the dHOPM algorithm where all modes are constricted. The analytical formulae derived from hypersquare tensors demonstrate that the best parallel performance is obtained when the splitting breaks the contiguity of tensor elements, in contrast to a naive approach that seeks to preserve this property for simplicity.

Numerical experiments of dTVC and dHOPM₃ algorithms have been carried out on three different architectures featuring CPUs, GPUs, and high-end memory, using native and looped (cuBLAS-based) implementations. On CPUs, we obtain dTVC bandwidth figures about 50% to 80% of the theoretical peak using up to 128 MPI processes, which are on par with those reported by the popular STREAM benchmark on a single NUMA node. In the case of dHOPM₃, figures are slightly lower, but overall they follow the same trend and, in absolute terms, the average throughput (kernel invocations per second) is, as expected, roughly half of that of dTVC regardless of the tensor order. On GPUs, the looped dTVC algorithm with state-of-the-art CUDA kernels brings an excess of variability into the results and, more importantly, evidences performance issues related to low device occupancy and increasing synchronous communication. In this regard, general-purpose computers are still able to compete against newer architectures equipped with low-capacity HBM or GPUs on strong scalability scenarios. Lastly, it has been proved that the use of mixed precision kernels with our proposed caching technique is an effective way of almost doubling or even quadrupling the throughput of dTVC and dHOPM algorithms, although the real performance may remain architecture-dependent.

Future work will focus on the development of a CUDA-based, native TVC kernel for GPUs following the same philosophy adopted in our CPU library. This will enable beyond state-of-the-art dTVC performance, and subsequently dHOPM performance, on these accelerators. On the other hand, it will be worth assessing the effects of multidimensional tensor splitting and the incursion of tensor unfolding operations. Analytical formulae for hypersquare tensors and numerical experiments with fine-grain parallelization will shed light in the pros and cons of increasing the number of splitting dimensions. Finally, we will seek to integrate this work within already existing frameworks, e.g. by bringing dense multilinear algebra support to ALP.

Acknowledgements

This work was supported in part by MCIN/AEI/10.13039/501100011033 and ESF/10.13039/501100004895 [grant number RYC2019-027592-I], and in part by the HPC Technology Innovation Lab, a Barcelona Supercomputing Center and Huawei research cooperation agreement (2020-2022). This work has also benefited financially from the Severo Ochoa Centre of Excellence accreditation [grant number CEX2021-001148-S] funded by MCIN/AEI. The Programming Models research group at BSC-UPC received financial support from Departament de Recerca i Universitats de la Generalitat de Catalunya [grant number 2021 SGR 01007].

References

- [1] T. G. Kolda, B. W. Bader, Tensor decompositions and applications, *SIAM Review* 51 (2009) 455–500. doi:10.1137/0707011X.
- [2] C. G. Khatri, C. R. Rao, Solutions to some functional equations and their applications to characterization of probability distributions, *Sankhyā: The Indian Journal of Statistics, Series A* (1961-2002) 30 (1968) 167–180.
- [3] L. D. Lathauwer, B. D. Moor, J. Vandewalle, On the best rank-1 and rank-(R_1, R_2, \dots, R_N) approximation of higher-order tensors, *SIAM J. Matrix Anal. Appl.* 21 (2000) 1324–1342. doi:10.1137/S0895479898346995.
- [4] L. R. Tucker, Some mathematical notes on three-mode factor analysis, *Psychometrika* 31 (1966) 279–311. doi:10.1007/bf02289464.
- [5] R. A. Harshman, Foundations of the PARAFAC procedure: Models and conditions for an “explanatory” multi-model factor analysis, in: *UCLA Working Papers in Phonetics*, volume 16, 1970, pp. 1–84.
- [6] F. Pawłowski, B. Uçar, A. N. Yzelman, A multi-dimensional Morton-ordered block storage for mode-oblivious tensor computations, *Journal of Computational Science* 33 (2019) 34–44. doi:10.1016/j.jocs.2019.02.007.
- [7] F. Pawłowski, B. Uçar, A. N. Yzelman, High performance tensor–vector multiplication on shared-memory systems, in: *Parallel Processing and Applied Mathematics*, 2020, pp. 38–48. doi:10.1007/978-3-030-43229-4_4.
- [8] P. J. Martínez-Ferrer, A.-J. Nicholas Yzelman, V. Beltran, A native tensor-vector multiplication algorithm for high performance computing, *IEEE Transactions on Parallel and Distributed Systems* 33 (2022) 3363–3374. doi:10.1109/TPDS.2022.3153113.
- [9] K. Shin, B. Hooi, J. Kim, C. Faloutsos, Detecting group anomalies in tera-scale multi-aspect data via dense-subtensor mining, *Frontiers in Big Data* 3 (2021). doi:10.3389/fdata.2020.594302.
- [10] P. J. Martínez-Ferrer, dTVC library (version 1.0) [Computer software], Code Ocean, 2024. doi:10.24433/CO.8844920.v1.
- [11] E. Di Napoli, D. Fabregat-Traver, G. Quintana-Ortí, P. Bientinesi, Towards an efficient use of the BLAS library for multilinear tensor contractions, *Applied Mathematics and Computation* 235 (2014) 454–468. doi:https://doi.org/10.1016/j.amc.2014.02.051.
- [12] C. Basso, Design of a high-performance tensor-vector multiplication with BLAS, in: *Computational Science – ICCS 2019*, 2019, pp. 32–45. doi:10.1007/978-3-030-22734-0_3.
- [13] Z. Xianyi, W. Qian, Z. Yunquan, Model-driven level 3 BLAS performance optimization on Loongson 3A processor, in: *Proceedings of the 2012 IEEE 18th International Conference on Parallel and Distributed Systems*, 2012, pp. 684–691. doi:10.1109/ICPADS.2012.97.
- [14] F. G. Van Zee, R. A. van de Geijn, BLIS: A framework for rapidly instantiating BLAS functionality, *ACM Transactions on Mathematical Software* 41 (2015) 14:1–14:33.

- [15] A. Heinecke, G. Henry, M. Hutchinson, H. Pabst, LIBXSMM: Accelerating small matrix multiplications by runtime code generation, in: Proceedings of the International Conference for High Performance Computing, Networking, Storage and Analysis, 2016. doi:10.5555/3014904.3015017.
- [16] U. Kang, E. Papalexakis, A. Harpale, C. Faloutsos, Gigatensor: Scaling tensor analysis up by 100 times - algorithms and discoveries, in: Proceedings of the 18th ACM SIGKDD International Conference on Knowledge Discovery and Data Mining, 2012, pp. 316–324. doi:10.1145/2339530.2339583.
- [17] N. Park, B. Jeon, J. Lee, U. Kang, BIGtensor: Mining billion-scale tensor made easy, in: Proceedings of the 25th ACM International on Conference on Information and Knowledge Management, 2016, pp. 2457–2460. doi:10.1145/2983323.2983332.
- [18] Z. Blanco, B. Liu, M. M. Dehnavi, CSTF: Large-scale sparse tensor factorizations on distributed platforms, in: Proceedings of the 47th International Conference on Parallel Processing, 2018. doi:10.1145/3225058.3225133.
- [19] D. W. Walker, The design of a standard message passing interface for distributed memory concurrent computers, *Parallel Computing* 20 (1994) 657–673. doi:10.1016/0167-8191(94)90033-7.
- [20] A. N. Yzelman, D. Di Nardo, J. M. Nash, W. J. Suijlen, A C++ GraphBLAS: specification, implementation, parallelisation, and evaluation, 2020. arXiv:1906.03196.
- [21] B. Brock, A. Buluç, T. Mattson, S. McMillan, J. Moreira, The GraphBLAS C API specification (Version 2.0.0) [Computer software], 2021. URL: https://graphblas.org/docs/GraphBLAS_API_C_v2.0.0.pdf.
- [22] D. G. Spampinato, D. Jelovina, J. Zhuang, A.-J. N. Yzelman, Towards structured algebraic programming, in: Proceedings of the 9th ACM SIGPLAN International Workshop on Libraries, Languages and Compilers for Array Programming, 2023, pp. 50–61. doi:10.1145/3589246.3595373.
- [23] E. Solomonik, D. Matthews, J. R. Hammond, J. F. Stanton, J. Demmel, A massively parallel tensor contraction framework for coupled-cluster computations, *Journal of Parallel and Distributed Computing* 74 (2014) 3176–3190. doi:10.1016/j.jpdc.2014.06.002.
- [24] J. A. Calvin, C. A. Lewis, E. F. Valeev, Scalable task-based algorithm for multiplication of block-rank-sparse matrices, in: Proceedings of the 5th Workshop on Irregular Applications: Architectures and Algorithms, 2015. doi:10.1145/2833179.2833186.
- [25] A. N. Ziogas, G. Kwasniewski, T. Ben-Nun, T. Schneider, T. Hoefler, Deinsum: Practically I/O optimal multi-linear algebra, in: SC22: International Conference for High Performance Computing, Networking, Storage and Analysis, 2022, pp. 1–15. doi:10.1109/SC41404.2022.00030.
- [26] E. Anderson, Z. Bai, C. Bischof, S. Blackford, J. Demmel, et al., LAPACK Users' Guide: Third Edition, 1999.
- [27] J. Dongarra, P. Luszczek, ScaLAPACK, 2011, pp. 1773–1775. doi:10.1007/978-0-387-09766-4_151.
- [28] J. Dongarra, I. Duff, M. Gates, A. Haidar, S. Hammarling, et al., A proposed API for batched basic linear algebra subprograms, MIMS EPrint 2016.25, The University of Manchester (2016).
- [29] E. Chan, M. Heimlich, A. Purkayastha, R. van de Geijn, Collective communication: theory, practice, and experience, *Concurrency and Computation: Practice and Experience* 19 (2007) 1749–1783. doi:<https://doi.org/10.1002/cpe.1206>.
- [30] L. Dagum, R. Menon, OpenMP: An industry standard API for shared-memory programming, *IEEE Computational Science and Engineering* 5 (1998) 46–55. doi:10.1109/99.660313.
- [31] J. M. Perez, V. Beltran, J. Labarta, E. Ayguadé, Improving the integration of task nesting and dependencies in OpenMP, in: IEEE International Parallel and Distributed Processing Symposium (IPDPS), 2017, pp. 809–818. doi:10.1109/IPDPS.2017.69.
- [32] J. D. McCaLpin, Memory bandwidth and machine balance in current high performance computers, *IEEE Computer Society Technical Committee on Computer Architecture Newsletter* (1995) 19–25.
- [33] P. J. Martinez-Ferrer, T. Arslan, V. Beltran, Improving the performance of classical linear algebra iterative methods via hybrid parallelism, *Journal of Parallel and Distributed Computing* 179 (2023) 104711. doi:10.1016/j.jpdc.2023.04.012.
- [34] S. Gupta, A. Agrawal, K. Gopalakrishnan, P. Narayanan, Deep learning with limited numerical precision, in: Proceedings of the 32nd International Conference on International Conference on Machine Learning - Volume 37, 2015, pp. 1737–1746.
- [35] D. Kalamkar, D. Mudigere, N. Mellempudi, D. Das, K. Banerjee, et al., A study of bfloat16 for deep learning training (2019). doi:10.48550/arxiv.1905.12322.
- [36] C. Rau, IEEE 754-based half-precision floating-point library (Version 2.2) [Computer software], SourceForge, 2023. URL: <https://half.sourceforge.net>.